

The Intrinsic Shapes of Low-Surface-Brightness Dwarf Irregular Galaxies and Comparison to Other Types of Dwarf Galaxies

Eon-Chang Sung

Korea Astronomy Observatory, Taejon, Korea 305-348,
Department of Astronomy, Yonsei University, Seoul, Korea 120-749
ecsung@hanul.issa.re.kr,

Cheongho Han

Department of Astronomy & Space Science,
Chungbuk National University, Cheongju, Korea 361-763
cheongho@astro-3.chungbuk.ac.kr,

Barbara S. Ryden

Department of Astronomy, The Ohio State University, Columbus, OH 43210
ryden@astronomy.ohio-state.edu,

Richard J. Patterson

Astronomy Department, University of Virginia, Charlottesville, VA, 22903
ricky@virginia.edu,

Mun-Suk Chun

Department of Astronomy, Yonsei University, Seoul, Korea 120-749
mschun@galaxy.yonsei.ac.kr,

Woo-Baik Lee

Korea Astronomy Observatory, Taejon, Korea 305-348
wblee@hanul.issa.re.kr,

Dong-Jin Kim

Department of Astronomy & Space Science,
Chungbuk National University, Cheongju, Korea 361-763
cheongho@astro-3.chungbuk.ac.kr,

Received _____; accepted _____

ABSTRACT

In this paper, we measure the ellipticities of 30 LSB dI galaxies and compare the ellipticity distribution with that of 80 dEs (Ryden & Terndrup 1994; Ryden et al. 1998) and 62 BCDs (Sung et al. 1998). We find that the ellipticity distribution of LSB dIs is very similar to that of BCDs, and marginally different from that of dEs. We then determine the distribution of intrinsic shapes of dI galaxies and compare to those of other type dwarf galaxies under various assumptions. First, we assume that LSB dIs are either all oblate or all prolate, and use non-parametric analysis to find the best-fitting distribution of intrinsic shapes. With this assumption, we find that the scarcity of nearly circular LSB dIs implies, at the 99% confidence level, that they cannot be a population of randomly oriented oblate or prolate objects. Next, we assume that dIs are triaxial, and use parametric analysis to find permissible distributions of intrinsic shapes. We find that if the intrinsic axis ratios, β and γ , are distributed according to a Gaussian with means β_0 and γ_0 and a common standard deviation of σ , the best-fitting set of parameters for LSB dIs is $(\beta_0, \gamma_0, \sigma) = (0.66, 0.50, 0.15)$, and the best fit for BCDs is $(\beta_0, \gamma_0, \sigma) = (0.66, 0.55, 0.16)$, while the best fit for dEs is $(\beta_0, \gamma_0, \sigma) = (0.78, 0.69, 0.24)$. The dIs and BCDs thus have a very similar shape distribution, given this triaxial hypothesis, while the dEs peak at a somewhat more spherical shape. Our results are consistent with an evolutionary scenario in which the three types of dwarf galaxy have a close relation with each other.

Subject headings: galaxies: dwarf irregulars – galaxies: blue compact dwarf – galaxies: dwarf elliptical – galaxies: structure

submitted to *The Astrophysical Journal*: ??? ??, 1998
Preprint: CNU-A&SS-01/98

1. Introduction

Although the faint end of the galaxy luminosity function is not well determined, recent studies indicate that low-surface-brightness (LSB) dwarf galaxies are by far the most numerous type of galaxy, and contribute a significant fraction of the mass of the universe (Reaves 1983; Binggeli, Sandage, & Tammann 1985; Phillipps et al. 1987). Morphologically, dwarf galaxies, like their counterpart bright galaxies, are classified into several types. The most common type of dwarf galaxy ($\sim 80\%$ of the total) is the dwarf elliptical (dE). These galaxies have regular elliptical isophotes and roughly exponential surface brightness profiles; they are often found in groups and clusters (Davies et al. 1988). The second type of dwarf galaxy is the blue compact dwarf (BCD) galaxy. In contrast to gas-poor dEs, BCDs contain giant HII regions surrounding O and B stars within a massive HI reservoir; BCDs exhibit spectra slowly rising toward the blue, implying that they are undergoing intense star formation (du Puy 1970; Searle & Sargent 1972). Most BCDs have regular isophotes in the outer region, like dEs, but the inner isophotes are frequently distorted from ellipses, due to the presence of bright HII regions (Loose & Thuan 1986).

The final type of dwarf galaxy is the LSB dwarf galaxy. LSB dwarfs include both irregular (dI) and more regular spiral (dS) galaxies. Like BCDs, they contain a large amount of HI, often with small OB associations, and have blue colors ($B - V \sim 0.5$ mag), indicating a significant level of recent star formation (Staveley-Smith, Davies, & Kinman 1992). However, they are distinguished from BCD galaxies by their amorphous shapes even in the outer region. Additionally, in contrast to dEs, these galaxies are more likely to be found outside of clusters (Bingelli, Tarenghi, & Sandage 1990).

The evolutionary connections among the three different types of dwarf galaxies remain both elusive and confusing. There are two major competing hypotheses for the evolutionary connection between BCDs and dEs. The first hypothesis claims that BCDs are basically a different population from dEs, as evidenced by the spectroscopic and spectrophotometric differences. According to this scenario, BCDs are truly young systems, in which the present star burst is the first in the galaxy's lifetime. The second hypothesis suggests that BCDs, like dEs, are mainly composed of old stellar populations, and that their observed spectroscopic features and spectral energy distributions are the result of a recent burst of star formation (Staveley-Smith et al. 1992). As an evidence for the second scenario, it is argued that the near-infrared emission in the vast majority of BCDs is attributable to old K and M giants, which are the major component of dEs (Thuan 1983; Hunter & Gallagher 1985).

Similarly, there exist two competing hypotheses to explain the evolutionary connection between dIs and dEs. The first hypothesis states that dE galaxies are the faded remnants of previously actively star-forming dI galaxies whose gas has been lost. There exists circumstantial evidence that dEs have in fact evolved directly from dIs. Faber & Lin (1983) and Kormendy (1985) have used the similarity in the surface brightness profiles of dIs and dEs, which are mostly exponential, to argue that gas-rich dIs are the progenitors of dEs. The second hypothesis for the relation between dIs and dEs states that they represent

parallel sequences of dwarf galaxies, fundamentally separated by the intrinsic difference in their structure. The observational evidence for this hypothesis is based mostly on the differences in appearance between the two types of dwarf galaxies; for instance, dIs have a more diffuse light distribution than dEs, and lack the bright nucleation which is frequently found in dEs. In addition to these differences, there is a dissimilarity in the flattening distribution of dEs and dIs; the apparent flattening of a galaxy is customarily given either by the apparent axis ratio q or by the ellipticity $\epsilon \equiv 1 - q$. Bothun et al. (1986) and Impey & Bothun (1997) presented the results of Ichikawa, Wakamatsu, & Okamura (1986) and Caldwell (1983) as evidence for the different flattening distributions between dEs and dIs. However, the analysis of Ichikawa et al. was based on the comparison between the flattening distributions of dEs and bright (non-dwarf) spiral galaxies; the situation is similar for Caldwell's analysis. In addition, contrary to the claims of Bothun et al. and Impey & Bothun, both Ichikawa et al. and Caldwell showed that the flattening distribution of dEs is similar to that of bright irregular galaxies.

There have been previous attempts to compare the apparent axis ratio distributions between LSB dI galaxies and other types of dwarf galaxies. For example, Staveley-Smith et al. (1992) constructed the axis ratio distribution for 438 Uppsala Galaxy Catalogue (hereafter UGC, Nilson 1973) LSB galaxies, and compared it to that of BCDs whose ellipticities were measured from Palomar Observatory Sky Survey (POSS) plates by Gorden & Gottesman (1981). However, previous studies of axis ratio distributions suffer from large uncertainties for several reasons. First, owing to the small dimensions and low surface brightness of dwarf galaxies, estimating their axis ratio is difficult and leads to large uncertainties. Second, the UGC sample used by Staveley-Smith et al. (1992) is known to be inhomogeneous, containing galaxies ranging from true dwarf galaxies to more luminous very low surface brightness systems (Thuan & Seitzer 1979; McGaugh, Schombert, & Bothun 1995). Finally, previous determinations of LSB dI axis ratios have been based on photographic plates; for comparison with recent CCD observations of other types of dwarf galaxy, it is essential to have measurements of the axis ratios of a homogeneous sample of LSB dIs based on modern CCD observations.

In this paper, we measure the ellipticities of 30 LSB dI galaxies and compare the ellipticity distribution with that of 80 dEs (Ryden & Terndrup 1994; Ryden et al. 1998) and 62 BCDs (Sung et al. 1998). We find that the ellipticity distribution of LSB dIs is very similar to that of BCDs, and marginally different from that of dEs. We then determine, under various assumptions, the distribution of intrinsic shapes of dI galaxies and compare it to that of other types of dwarfs. First, we assume that LSB dIs are either all oblate or all prolate, and use non-parametric analysis to find the best-fitting distribution of intrinsic shapes. With this assumption, we find that the scarcity of nearly circular LSB dIs implies, at the 99% confidence level, that they cannot be a population of randomly oriented oblate or prolate objects. Next, we assume that dIs are triaxial, and use parametric analysis to find permissible distributions of intrinsic shapes. We find that if the intrinsic axis ratios, β and γ , are distributed according to a Gaussian with means β_0 and γ_0 and a common standard deviation of σ , the best-fitting set of parameters for LSB dIs is

$(\beta_0, \gamma_0, \sigma) = (0.66, 0.50, 0.15)$, and the best fit for BCDs is $(\beta_0, \gamma_0, \sigma) = (0.66, 0.55, 0.16)$, while the best fit for dEs is $(\beta_0, \gamma_0, \sigma) = (0.78, 0.69, 0.24)$. The LSB dIs and BCDs thus have a very similar shape distribution, given this triaxial hypothesis, while the dEs peak at a somewhat more spherical shape. Our results are consistent with an evolutionary scenario in which the three types of dwarf galaxy have a close relation with each other.

2. Observations

Our sample consists of 30 LSB dI galaxies which are drawn from the list of UGC “dwarfs” and LSB galaxies detected in HI by Schneider et al. (1990; 1992). In the UGC catalogue, “dwarfs” are categorized as “objects with very low surface brightness and little or no concentration of light on the red prints” with Hubble types of Sc-Irr or later (Nilson 1973). Among these galaxies, we select only galaxies with small 21 cm HI line widths, $\Delta v_{20} \leq 100 \text{ km s}^{-1}$, small redshifts, $v_0 \leq 1,500 \text{ km s}^{-1}$, and faint B -band luminosities, $M_B \gtrsim -16$. For galaxies not observed by Schneider et al. (1992), HI data were taken from Huchtmeier & Richter (1989). In addition, we exclude galaxies with noticeable spiral patterns so that the sample is composed of pure dwarf irregular galaxies. In POSS prints, most galaxies in our sample are found to be of generally low surface brightness, with superimposed irregular patches of star formation.

The photometric observations of the sample galaxies were carried out during several observing runs from 1985 to 1993 with different CCD chip and telescope combinations; by using the KPNO 4 m with a 320×512 RCA1 chip during 1995 May 22–23, the KPNO 2.1 m with a 512×512 T5HA chip during 1990 October 19–22 and 1991 April 17–21, the 2.1 m with a 1024×1024 T1KA chip during 1993 January 23–24, the KPNO 0.9 m with a 1024×1024 ST1K chip during 1991 September 13–16, and the 0.9 m with a 1024×1024 T2KA chip during April 18–20. The galaxy names and observed bands are listed in Table 1; images of individual galaxies were presented in Figure 2 of Patterson & Thuan (1996).

All steps of the data reduction and analysis were carried out using a standard CCD reduction process with IRAF¹. First, a bias offset was subtracted from each raw frame. To compensate for pixel-to-pixel variations in the bias level, we constructed a composite zero frame of 20 individual bias frames (with the overscan already subtracted), and subtracted it from each frame. Next, images were divided by the combined flat images constructed from high signal-to-noise level dome and sky flats for individual nights to remove the pixel-to-pixel variation in the detector sensitivity. Then, blank dark sky exposures were used to remove the interference pattern produced by night sky emission lines. Finally, after individual object frames were processed through the flat fielding correction, separate

¹IRAF is distributed by National Optical Astronomy Observatories, which is operated by the Association of Universities for Research in Astronomy, Inc., under cooperative agreement with the National Science Foundation.

exposure were aligned and combined, followed by sky subtraction. Further details of the data reduction can be found in Patterson & Thuau (1996).

3. Axis Ratio Determination

We determine the apparent axis ratios of individual LSB dIs by fitting ellipses to the isophotes of obtained images. For this process, the most widely used program is the Space Telescope Science Data Analysis System (STSDAS) routine “isophote”, which is based on an iterative least-square fit to a Fourier expansion. However, since the routine is designed for fitting the surface brightness distributions of stellar systems with uniform profiles, such as elliptical galaxies, it often produces an unstable fit when it is used for spirals and irregular galaxies (Freudling 1992). Therefore, we take a different approach which utilizes a fully two-dimensional linear fit of the harmonics to the image. In this approach, the intensity of a galaxy is parameterized as a series of harmonic terms by

$$I(a, \psi) = \sum_{n=0}^k I_n(a) \cos \{n [\psi - \psi_n(a)]\}, \quad (3.1)$$

where ψ is the position angle with respect to the major axis of the ellipse (Franx, Illingworth, & Heckman 1989). The results of harmonic fits are then used as the initial values for the usual Fourier series expansion ellipse fitting routine, “isophote”. Due to the small angular size of our images we allowed the program to fit ellipses up to the radius at which only 60% of points on the ellipse lay within the image. The center and position angle of the isophotes were generally allowed to vary. During the fitting process we excluded HII regions within the galaxy from each image along with foreground stars and cosmic rays. The measured ellipticity profiles of individual galaxies were presented in Figures 64-71 of Patterson (1995).

The axis ratios of the LSB dI galaxies in our sample, like those of many stellar systems, vary as a function of semimajor axis. We find that the variation is most severe in the inner parts, and is mostly caused by the existence of irregular structures. In the outer parts, on the other hand, the ellipse-fitting process fails as the surface brightness falls far below the sky brightness. Therefore, as a representative axis ratio we determine the intensity-weighted axis ratio averaged over the intermediate region where we could obtain stable values of axis ratios with successful ellipse-fitting process. The intensity-weighted mean axis ratio is computed by

$$\bar{q} = \frac{\int q(a) dL}{\int dL}; \quad dL = 2\pi qa \left[1 + \frac{1}{2} \frac{d\ln q(a)}{d\ln a} \right] \Sigma(a) da, \quad (3.2)$$

where $q = b/a$, a is the semimajor axis of the isophote, b is the semiminor axis, and $\Sigma(a)$ is the surface brightness of the isophote with semimajor axis a . In Table 1 we present the finally determined mean ellipticities, $\bar{\epsilon} \equiv 1 - \bar{q}$, and their uncertainties. The errors are estimated by computing the variance of $q(a)$ within the range of semimajor axes where ellipticities are measured.

Due to the variation of axis ratios within a galaxy, it is important to apply a consistent method of ellipticity determination for the comparison between different types of galaxies. Since the mean ellipticities for the dE sample of Ryden & Terndrup (1994) and Ryden et al. (1998) and those for BCDs of Sung et al. (1998) were determined adopting the same method for similarly obtained CCD data, we can directly compare the axis ratio distribution of LSB dIs with the other types of dwarf galaxies. In the upper panel of Figure 1, we present the cumulative function of \bar{q} for 30 LSB dIs in our sample (solid step function), and compare it with those of 80 dE and 62 BCD samples. From this comparison, we find that the axis ratio distribution of LSB dIs is very similar to that of BCDs; the Kolmogorov-Smirnov (hereafter KS) probability for comparing these two samples is $P_{\text{KS}} = 0.70$. Compared to dEs, LSB dIs are slightly flatter, on average. For the sample of LSB dIs the mean and standard deviation of \bar{q} are 0.64 ± 0.15 , while those for the dE sample are 0.70 ± 0.16 . However, the difference in the axis ratio distributions between these two samples is marginal with a KS probability of $P_{\text{KS}} = 0.060$. The results of comparing the apparent axis ratio distributions between the different types of dwarf galaxies are summarized in Table 2.

4. Determining Intrinsic Shapes

For the determination of intrinsic shapes, we apply two different methods: non-parametric and parametric. The non-parametric method assumes that the galaxies in a sample are either all oblate or all prolate, with intrinsic axis ratio γ , and are randomly oriented relative to us. With these assumptions, the distribution $f(\gamma)$ of intrinsic shapes can be determined from the distribution $f(q)$ of apparent shapes by performing a unique mathematical inversion. The parametric method, by contrast, assumes that the galaxies are triaxial, with axis lengths in the ratio $1 : \beta : \gamma$, where $1 \geq \beta \geq \gamma$. In this case, there is no longer a unique inversion from the observed distribution $f(q)$ to the intrinsic distribution $f(\beta, \gamma)$. However, using a parametric model for $f(\beta, \gamma)$, we can find the model distribution of intrinsic axis ratios which best fits the observed distribution of apparent axis ratios. Compared to the first method, the parametric method has the disadvantage that one has to assume a functional form (e.g., Gaussian) for the model axis ratio distribution, which is actually poorly known. Nevertheless, parametric fits are useful because they show us how statistics such as the KS and χ^2 scores vary as the parameters are changed.

4.1. Non-parametric Method

If all LSB dI galaxies were randomly oriented oblate spheroids and if we knew exactly the distribution of apparent shapes $f(q)$, then we could perform a mathematical inversion on $f(q)$ to find the distribution $f_o(\gamma)$ for the intrinsic axis ratios of the oblate spheroids. Unfortunately, we don't know $f(q)$; we only have a sample of finite size drawn from the distribution. Thus, we can only accept or reject, at a known confidence level, the null hypothesis that the galaxies in the sample are randomly oriented oblate spheroids. In

addition, if the null hypothesis is not rejected, we can present an estimate of the distribution function $f_o(\gamma)$. In a similar way, we can accept or reject the hypothesis that the galaxies in the sample are randomly oriented prolate spheroids.

To test the oblate and prolate hypotheses, we start by making a non-parametric kernel estimate of the distribution $f(q)$ of the apparent axis ratios. Details of how non-parametric kernel estimators are used in this context are given by Tremblay & Merritt (1995) and Ryden (1996). We then numerically invert our estimate for $f(q)$ to find estimates for $f_o(\gamma)$ and $f_p(\gamma)$, the distributions of intrinsic axis ratios given the oblate and prolate hypotheses, respectively. Confidence intervals are placed on the estimates for f , f_o , and f_p by performing repeated bootstrap resampling of the original data set and creating new estimates from each bootstrap resampling. The spread in the bootstrap estimates of f at a given value of q , and in the bootstrap estimates of f_o and f_p at a given value of γ , provides confidence intervals for the non-parametric estimates of these functions. Once the estimates for f_o and f_p are determined, we can reject the oblate or prolate hypothesis at a given confidence level if the upper confidence level drops below zero for any value of the intrinsic axis ratio γ . (A hypothesis that calls for a negative number of galaxies at a given axis ratio is unphysical, and should be firmly rejected.)

In the upper panel of Figure 2, we present the non-parametric kernel estimate of the distribution of the apparent axis ratios \bar{q} for our sample of 30 LSB dIs. In the middle panel, we show the distribution of intrinsic axis ratios assuming the LSB dIs are oblate; in the lower panel, we show the distribution of intrinsic axis ratios assuming they are prolate. In each panel, the solid line is the best estimate, the dashed lines show the 80% confidence band, and the dotted lines show the 98% confidence band. (That is, at a given value of q , 1% of the bootstrap estimates fall above the upper boundary of the 98% confidence band, and 1% fall below the lower boundary of the 98% confidence band.) A Gaussian kernel was used to ensure a smooth, differentiable estimate of f , with a width $h = 0.069$. Because we imposed a more-or-less arbitrary reflective boundary condition at $q = 1$, we don't believe our estimates for f , f_o , and f_p , within a distance $\sim h$ of the right-hand edge of Figure 2.

Note that there is a decided lack of nearly circular LSB dIs in our sample; the roundest galaxy we observed has $q = 0.873$. This scarcity of nearly circular galaxies is the characteristic sign that the galaxies cannot be a population of oblate spheroids. Looking at the middle panel, we see that the oblate hypothesis can be ruled out at the 99% (one-sided) confidence level. The 98% confidence band for f_o drops below zero for axis ratios $\gamma > 0.85$. Indeed, so pronounced is the lack of nearly circular galaxies, even the prolate hypothesis can be ruled out at the 99% (one-sided) confidence level. The 98% confidence band for f_p drops below zero for $\gamma > 0.90$. Thus, even with our relatively small sample of galaxies, we can reject at a high confidence level the hypothesis that the LSB dI galaxies are a population of randomly oriented spheroids, either oblate or prolate. This leads us to consider, in the next section, possible distributions of triaxial shapes for the LSB dI galaxies in our sample.

4.2. Parametric Method

To determine the intrinsic axis ratio distribution of LSB dI galaxies, we model the distribution of intrinsic axis ratios (β, γ) as a Gaussian distribution with means β_0 and γ_0 and a common width σ ; i.e.,

$$f(\beta, \gamma) \propto \exp \left[-\frac{(\beta - \beta_0)^2 + (\gamma - \gamma_0)^2}{2\sigma^2} \right]. \quad (4.2.1)$$

We then produce a large number ($\sim 10^5$) of test galaxies with their intrinsic axis ratios distributed according to equation (4.2.1), and with random orientations with respect to us. Once test galaxies are produced, we then compute their projected axis ratio q . When a triaxial ellipsoid is projected with the viewing angles of θ and ϕ , it appears as an ellipse with an apparent axis ratio of

$$q(\beta, \gamma, \theta, \phi) = \left[\frac{A + C - \sqrt{(A - C)^2 + B^2}}{A + C + \sqrt{(A - C)^2 + B^2}} \right]^{1/2}, \quad (4.2.2)$$

where

$$\begin{cases} A = (\cos^2 \phi + \beta^2 \sin^2 \phi) \cos^2 \theta + \gamma^2 \sin^2 \theta, \\ B = \cos \theta \sin 2\phi (1 - \beta^2), \\ C = \sin^2 \phi + \beta^2 \cos^2 \phi \end{cases} \quad (4.2.3)$$

(Binney 1985). We then statistically compare the projected axis ratio distribution of test galaxies with the observed one using a KS test (for the cumulative distribution) and χ^2 test (for the binned distribution).

In Figure 3a and 3b, we present the isoprobability contours on 6 slices through the $(\beta_0, \gamma_0, \sigma)$ parameter space, as measured by KS and χ^2 tests, respectively, for our LSB dI sample. When measured by a KS test, the best-fitting distribution has parameters of $(\beta_0, \gamma_0, \sigma) = (0.66, 0.50, 0.15)$ with the KS probability $P_{\text{KS}} = 0.98$, implying that the intrinsic shape of LSB dIs can be well fitted by a population of triaxial ellipsoids. We obtain consistent results when measured by χ^2 tests; the best-fitting distribution has parameters of $(\beta_0, \gamma_0, \sigma) = (0.80, 0.42, 0.20)$ with the χ^2 probability $P_{\chi^2} = 0.91$.

For the comparison with other types of dwarf galaxies, we list the parameters of the best-fitting distributions for BCDs and dEs in Table 2. The isoprobability contours from which these parameters are drawn, were presented in Fig 6a, 6b, and 7 of Sung et al. (1998). In addition, in the lower panel of Figure 1 we present the computed cumulative distribution (smooth curve) for the best-fitting triaxial model, as measured by the KS test. The best-fitting model is overlaid on the measured cumulative distribution (step function) for each type of dwarf galaxy.

5. Summary

We measure the ellipticities for a sample of 30 LSB dIs and compare the distribution of ellipticities with those for the samples of 62 BCDs and 80 dEs. From this comparison, we find that the axis ratio distribution of LSB dIs is very similar to that of BCDs. Compared to dEs, LSB dIs are slightly flatter, but the difference is marginal. We also determine the intrinsic shape of LSB dIs from the distribution of apparent axis ratios. From the non-parametric analysis, we find the hypothesis that our sample LSB dIs are randomly oriented oblate or prolate objects is rejected with strong confidence level. On the other hand, the shape of LBS dI galaxies are well described by triaxial spheroids if their axis ratios, β and γ , have a Gaussian distribution. From the parametric analysis, we determine the best-fitting parameters are $(\beta_0, \gamma_0, \sigma) = (0.66, 0.50, 0.15)$. These results directly contradict the long-standing belief that LSB dIs have very flattened disk-like shapes, quite different from the spheroidal shapes of dEs and BCDs. Therefore, our results are consistent with the scenario that the three major types of dwarf galaxies have very close evolutionary connections.

E.-C. S. has been supported by Basic Research Fund of Korea Astronomy Observatory. B. S. R. was supported by grant NSF AST-93-577396.

REFERENCES

Bingelli, B., Tarenghi, M., & Sandage, A. 1990, *A&AS*, 228, 42

Bingelli, B., Sandage, A., & Tammann, G. A. 1985, *AJ*, 90, 1681

Binney, J. 1985, *MNRAS*, 212, 767

Bothun, G. D., Mould, J. R., Caldwell, N., & MacGillivray, H. T. 1986, *AJ*, 92, 1007

Caldwell, N. 1983, *AJ*, 88, 804

Davies, J. I., Phillipps, S., Cawson, M. G. M., & Kibblewhite, E. J. 1988, *MNRAS*, 232, 239

du Puy, D. L. 1970, *AJ*, 75, 1143

Faber, S. M., & Lin, D. N. C. 1983, *ApJ*, 266, L17

Franx, M., Illingworth, G., & Heckman, T. 1989, *AJ*, 98, 538

Freudling, W. 1992, User's Manual, ESO

Gorden, D., & Gottesman, S. T. 1981, *AJ*, 86, 161

Huchtmeier, W. K., & Richter, O.-G. 1989, A General Catalog of HI Observations of Galaxies (New York: Springer-Verlag)

Hunter, D. A., & Gallagher, J. S 1985, *ApJS*, 58, 533

Ichikawa, S.-I., Wakamatsu, K.-I., & Okamura, S. 1986, *A&AS*, 60, 475

Impey, C., & Bothun, G. D. 1997, *ARA&A*, 35, 267

Jorgensen, I., Franx, M., & Kjargaard, P. 1992, *A&AS*, 95, 489

Kormendy, J. 1985, *ApJ*, 295, 73

Loose, H. H., & Thuan, T. X. 1986, in Star-Forming Galaxies and Related Objects, ed. D. Kunth, T. X. Thuan, & J. T. T. Van (Gif-sur-Yvette: Editions Frontières), 73

McGaugh, S. S., Schombert, J. M., & Bothun, G. D. 1995, *AJ*, 109, 2019

Nilson, P. 1973, Uppsala General Catalogue of Galaxies (Uppsala Astro. Obs. Ann. v6)

Patterson, R. J. 1995, Ph.D. Thesis, University of Virginia

Patterson, R. J., & Thuan, T. X. 1996, *ApJS*, 107, 103

Phillipps, S., Disney, M. J., Kibblewhite, E. J., & Cawson, M. G. M., 1987, *MNRAS*, 229, 505

Reaves, G. 1983, *ApJS*, 53, 375

Ryden, B. S., & Terndrup, D. M. 1994, *ApJ*, 425, 43

Ryden, B. S. 1996, *ApJ*, 461, 146

Ryden, B. S., Terndrup, D. M., Pogge, R. W., & Lauer, T. R. 1998, *ApJ*, submitted

Schneider, S. E., Thuan, T. X., Magri, C., & Wadiak, J. E. 1990, *A&AS*, 72, 245

Schneider, S. E., Thuan, T. X., Mangum, J. G., & Miller, J. 1992, *A&AS*, 81, 5

Searle, L., & Sargent, W. L. 1972, *ApJ*, 173, 25
Sung, E.-C., Han, C., Ryden, B. S., Chun, M. S., & Kim, H.-I. 1998, *ApJ*, 499, 000
Staveley-Smith, L., Davies, R. D., & Kinman, T. D. 1992, *A&AS*, 258, 334
Thuan, T. X. 1983, *ApJ*, 268, 667
Tremblay, B., & Merritt, D. 1995, *AJ*, 110, 1039
Thuan, T. X., & Seitzer, P. O. 1979, *ApJ*, 231, 680

TABLE 1
THE INTENSITY WEIGHTED MEAN ELLIPTICITIES

No.	galaxy name	obs. band	ellipticity $\bar{\epsilon} \pm \Delta\epsilon$	No.	galaxy name	obs. band	ellipticity $\bar{\epsilon} \pm \Delta\epsilon$
1	KARA 10	<i>I</i>	0.429 \pm 0.0809	16	UGC 04173	<i>I</i>	0.601 \pm 0.0082
2	M81dwA	<i>I</i>	0.159 \pm 0.3767	17	UGC 05423	<i>I</i>	0.375 \pm 0.0843
3	UGC 00031	<i>I</i>	0.271 \pm 0.1166	18	UGC 07548	<i>I</i>	0.471 \pm 0.1832
4	UGC 00063	<i>I</i>	0.421 \pm 0.0454	19	UGC 07596	<i>I</i>	0.568 \pm 0.0606
5	UGC 00300	<i>I</i>	0.182 \pm 0.1562	20	UGC 07636	<i>I</i>	0.304 \pm 0.0780
6	UGC 00772	<i>B</i>	0.426 \pm 0.0677	21	UGC 07684	<i>I</i>	0.368 \pm 0.0267
7	UGC 01171	<i>I</i>	0.383 \pm 0.0340	22	UGC 08091	<i>I</i>	0.333 \pm 0.3350
8	UGC 01981	<i>I</i>	0.163 \pm 0.0356	23	UGC 08201	<i>B</i>	0.243 \pm 0.3216
9	UGC 02017	<i>I</i>	0.434 \pm 0.1183	24	UGC 08683	<i>I</i>	0.415 \pm 0.1102
10	UGC 02034	<i>I</i>	0.127 \pm 0.2909	25	UGC 08760	<i>I</i>	0.758 \pm 0.1550
11	UGC 02053	<i>I</i>	0.629 \pm 0.2038	26	UGC 08833	<i>I</i>	0.251 \pm 0.0767
12	UGC 02162	<i>I</i>	0.245 \pm 0.1463	27	UGC 09128	<i>I</i>	0.481 \pm 0.0993
13	UGC 03212	<i>I</i>	0.587 \pm 0.1721	28	UGC 10031	<i>I</i>	0.283 \pm 0.2665
14	UGC 03817	<i>I</i>	0.297 \pm 0.3201	29	UGC 10669	<i>I</i>	0.227 \pm 0.1074
15	UGC 03966	<i>I</i>	0.250 \pm 0.1087	30	UGC 12894	<i>I</i>	0.277 \pm 0.0633

NOTE.— The intensity weighted mean ellipticities of 30 LSB dI galaxies and their uncertainties. The errors are estimated by computing the variance of $\epsilon(a)$ within the range of semimajor axis a where the ellipticities are measured. Also marked are the band of images for which the ellipticities are measured.

TABLE 2
COMPARISON OF ELLIPTICITY DISTRIBUTIONS

galaxy type	$\langle \bar{q} \rangle$		P_{KS}	
	type 1	type 2		
LSB dIs	0.64 ± 0.15	vs.	BCDs	0.701
BCDs	0.67 ± 0.15	vs.	dEs	0.057
dEs	0.72 ± 0.16	vs.	LSB dIs	0.060

NOTE.— Comparisons of observed axis ratio distributions between the different types of dwarf galaxies, as measured by KS test. The mean axis ratios $\langle \bar{q} \rangle$ are based on the samples of 30 LSB dIs from this paper, 62 BCDs from Sung et al. (1998), and 80 dEs from Ryden & Terndrup (1994) and Ryden et al. (1998).

TABLE 3
BEST-FITTING PARAMETERS

galaxy type	statistical test	best-fitting parameters			best-fitting statistics
		β_0	γ_0	σ	
LSB dIs	KS	0.66	0.50	0.15	$P_{\text{KS}} = 0.98$
	χ^2	0.80	0.42	0.20	$P_{\chi^2} = 0.91$
BCDs	KS	0.66	0.55	0.16	$P_{\text{KS}} = 0.99$
	χ^2	0.77	0.51	0.16	$P_{\chi^2} = 0.96$
dEs	KS	0.78	0.69	0.24	$P_{\text{KS}} = 0.99$
	χ^2	0.87	0.64	0.24	$P_{\chi^2} = 0.94$

NOTE.— Best-fitting parameters and statistics for intrinsic axis ratio distributions for the three different types of dwarf galaxies, as measured by KS and χ^2 tests. We assume that galaxies are triaxial ellipsoids with axis ratio $1 \leq \beta \leq \gamma$, and the distribution of intrinsic axis ratios follows a Gaussian distribution with means β_0 and γ_0 and a common width σ .

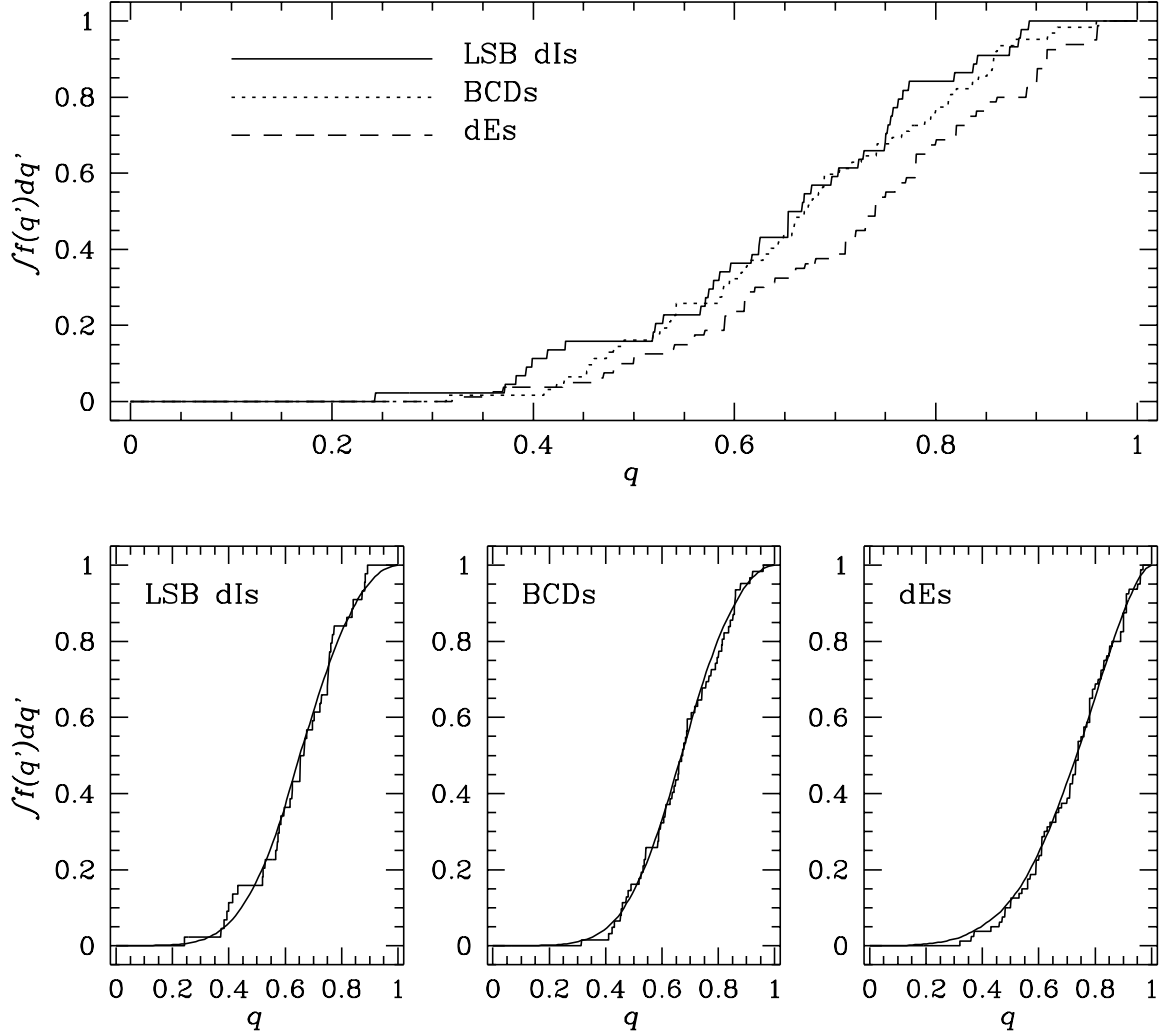


Figure 1: Upper panel: The cumulative distributions of apparent axis ratios for 30 LSB dIs (solid line), 62 BCDs (short-dashed line), and 80 dEs (long-dashed line). Lower panels: The cumulative distributions of apparent axis ratio distributions are superimposed on the predicted distributions of apparent shapes from the best-fitting triaxial models, as measured by KS tests.

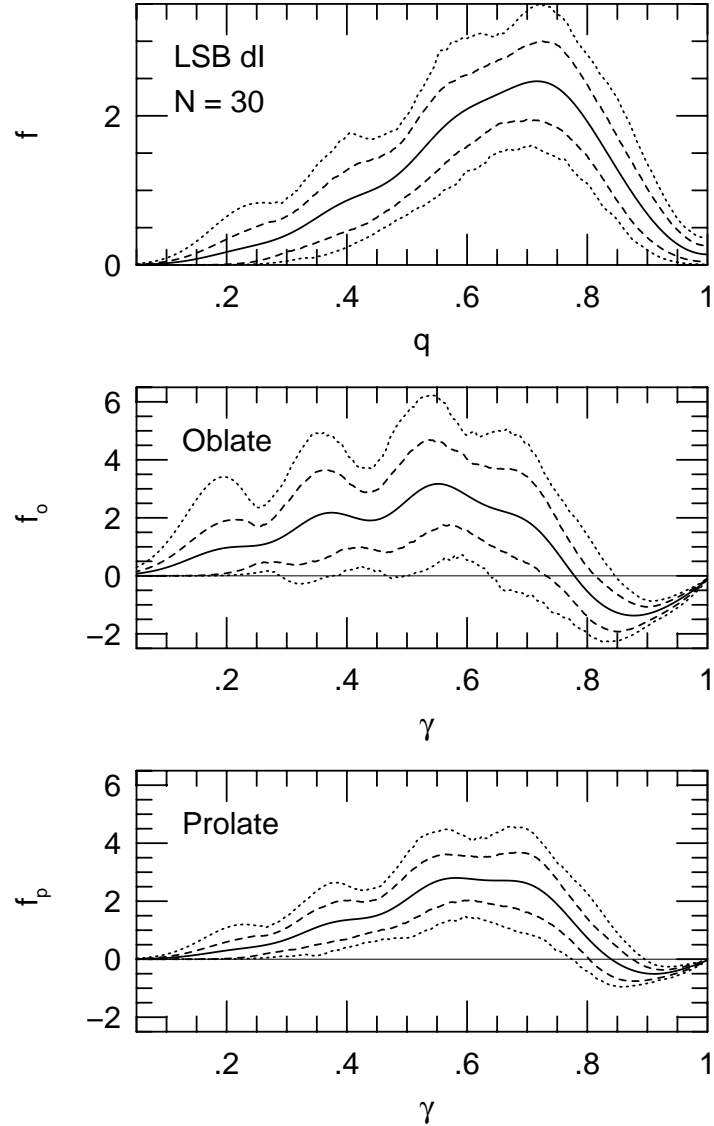


Figure 2: The non-parametric kernel estimate of the distribution of 30 LSB dI sample galaxies (top panel). Also shown are the distributions of intrinsic axis ratios, which are produced under the assumption that LSB dIs are all oblate (middle panel) and all prolate (bottom panel). The solid line in each panel is the best estimate, the dashed lines are the 80% confidence band, and dotted lines are the 98% confidence band.

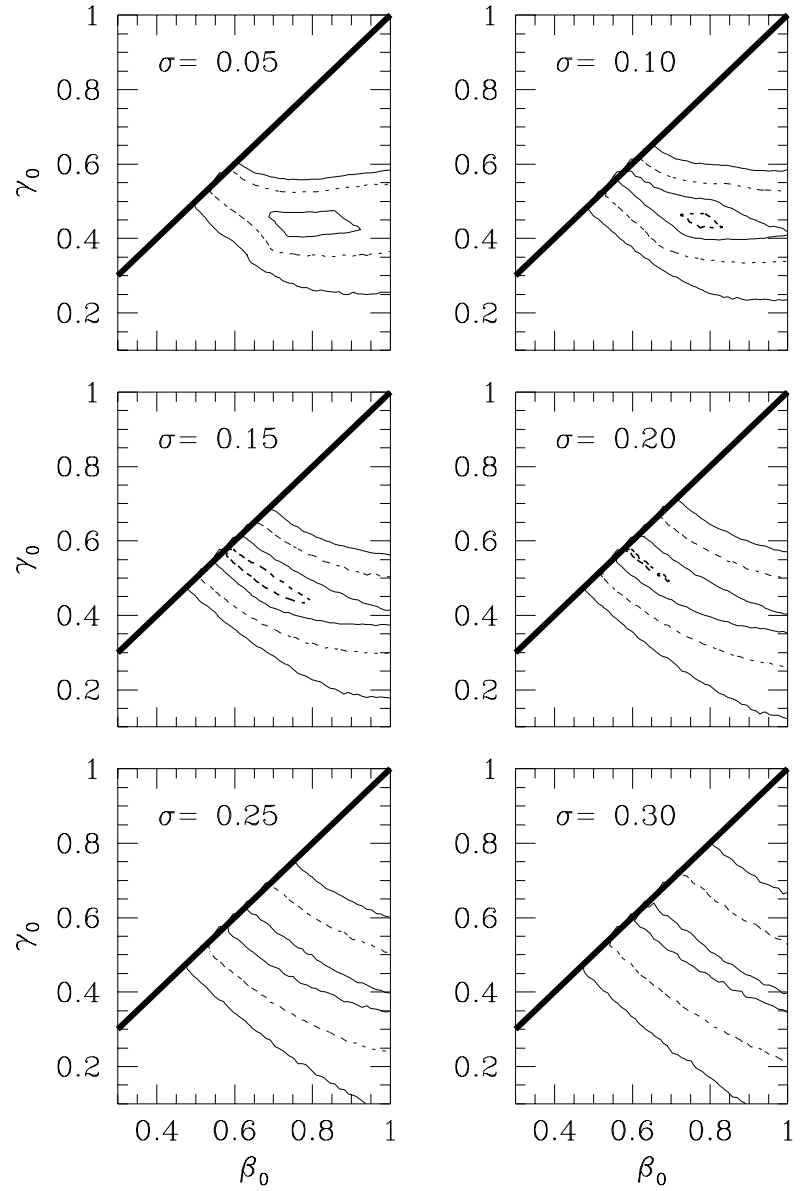


Figure 3a: The isoprobability contours, as measured by KS tests for 30 LSB dIs, on 6 slices through $(\beta_0, \gamma_0, \sigma)$ parameter space. Contours are drawn at the levels $P_{\text{KS}} = 0.01, 0.1, 0.5$, and 0.9, starting from the outside.

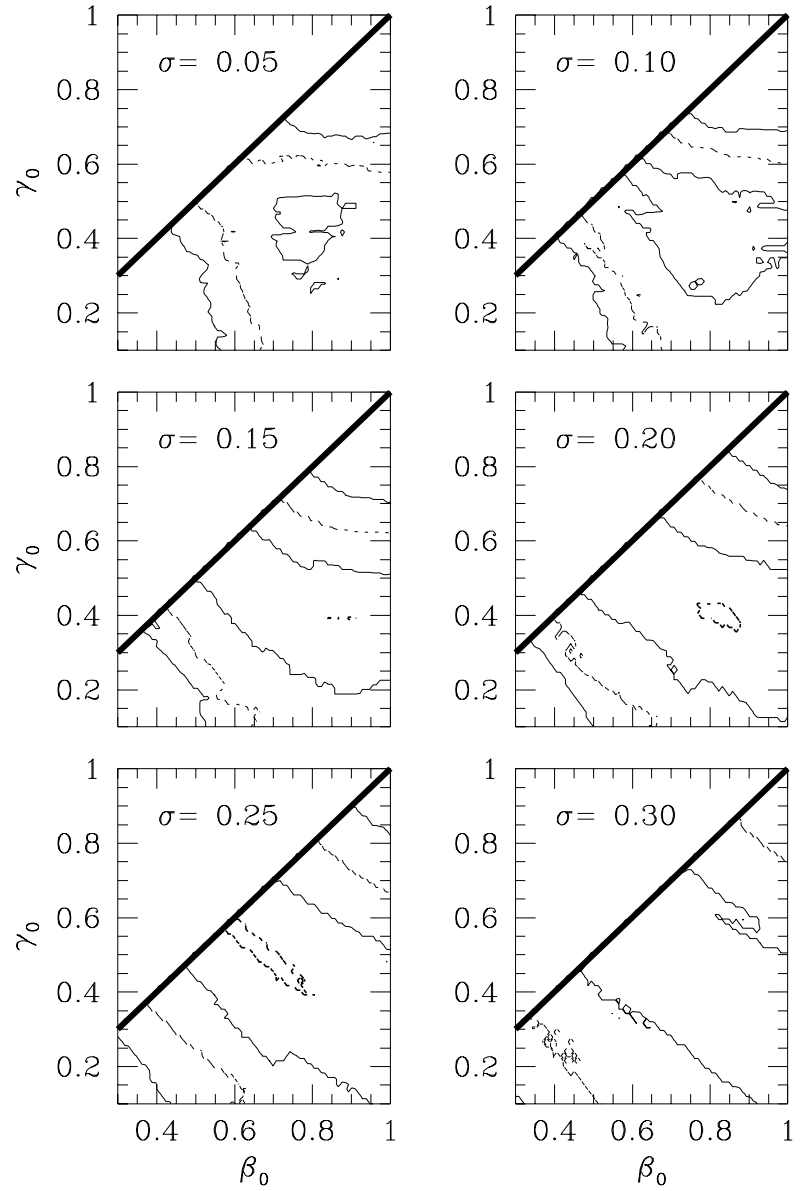


Figure 3b: The isoprobability contours, as measured by χ^2 tests for 30 LSB dIs, on 6 slices through $(\beta_0, \gamma_0, \sigma)$ parameter space. Contours are drawn at the levels $P_{\chi^2} = 0.01, 0.1, 0.5$, and 0.9, starting from the outside.